

Evidence for the coexistence of time-reversal symmetry breaking and Bardeen-Cooper-Schrieffer-like superconductivity in La_7Pd_3

D. A. Mayoh,^{1,*} A. D. Hillier,² G. Balakrishnan,¹ and M. R. Lees^{1,†}

¹*Physics Department, University of Warwick, Coventry, CV4 7AL, United Kingdom*

²*ISIS Facility, STFC Rutherford Appleton Laboratory,
Harwell Science and Innovation Campus, Oxfordshire OX11 0QX, United Kingdom*

Time-reversal symmetry breaking (TRSB) with a Bardeen-Cooper-Schrieffer (BCS) -like superconductivity occurs in a small, but growing number of noncentrosymmetric (NCS) materials, although the mechanism is poorly understood. We present heat capacity, magnetization, resistivity, and muon spin resonance/relaxation (μSR) measurements on polycrystalline samples of NCS La_7Pd_3 . Transverse-field μSR and heat capacity data show La_7Pd_3 is a type-II superconductor with a BCS-like gap structure, while zero-field μSR results provide evidence of TRSB. We discuss the implications of these results for both the La_7X_3 (where $X = \text{Ni}, \text{Pd}, \text{Rh}, \text{Ir}$) group of superconductors and other CS and NCS superconductors for which TRSB has been observed.

I. INTRODUCTION

The discovery of time-reversal symmetry breaking (TRSB) in polycrystalline La_7Ir_3 has provided a new group of superconductors in which to investigate unconventional superconducting behavior [1]. The report of an isotropic s -wave gap symmetry (nodeless) superconductivity in La_7Ir_3 , along with density functional theory calculations suggesting that the enhanced specific heat in this compound is due to electron-phonon coupling, have raised questions about the origin of the TRSB in this material [1, 2]. Time-reversal symmetry breaking has also been observed in La_7Rh_3 [3] suggesting this is a common feature of the La_7X_3 (where $X = \text{Ni}, \text{Pd}, \text{Rh}, \text{Ir}$) series. Here we present evidence of time-reversal symmetry breaking in La_7Pd_3 which further cements this claim.

Noncentrosymmetric (NCS) superconductors have garnered considerable interest in recent years. Their lack of a center of inversion means that parity is no longer a good quantum number [4]. A Rashba-type anti-symmetric spin-orbit coupling is allowed, lifting the degeneracy of the Fermi surface. The superconducting Cooper pairs may then form with a mixture of spin-singlet or spin-triplet components [5, 6]. The superconducting gap function Δ can be described by $\Delta = i\tilde{\sigma}_y [\psi(\mathbf{k}) + \mathbf{d}(\mathbf{k}) \cdot \tilde{\boldsymbol{\sigma}}]$, where for a pure singlet $\mathbf{d}(\mathbf{k}) = 0$ and the triplet case corresponds to $\psi(\mathbf{k}) = 0$. It is important to note that if the triplet term is small, there will be a nodeless, near isotropic gap, making it experimentally difficult to distinguish from a Bardeen-Cooper-Schrieffer (BCS) -like s -wave superconductor.

A noncentrosymmetric superconductor with a mixture of triplet and singlet states may be expected to display unconventional superconducting properties. A large number of NCS superconductors have now been studied and many have indeed been shown to exhibit exotic superconducting behavior [4, 7]. For example,

CePt_3Si , is an antiferromagnetic heavy fermion superconductor [8], BiPd , has an unconventional order parameter [9], $\text{Li}_2\text{Pt}_3\text{B}$, has a line-nodal gap structure [10–13], and $(\text{Ta/Nb})\text{Rh}_2\text{B}_2$, are multigap superconductors with upper critical fields that violate the Pauli limit [14–16].

The possibility of spin-triplet superconductivity or singlet-triplet mixing make NCS superconductors prime candidates to exhibit time-reversal symmetry breaking. Muon spectroscopy studies of several NCS superconductors, including LaNiC_2 [17] and several members of the Re_6T ($T = \text{Zr}, \text{Hf}, \text{Ti}$) α -Mn group of materials [18–22] have confirmed the presence of spontaneous magnetic moments that arise below the superconducting transition temperature, T_c , when time-reversal symmetry is broken [23]. However, TRSB has also been observed in a number of centrosymmetric superconductors such as Sr_2RuO_4 [24, 25], $\text{PrPt}_4\text{Ge}_{12}$ [26], $(\text{Pr},\text{La})(\text{Os},\text{Ru})_4\text{Sb}_{12}$ [27, 28], LaNiGa_2 [29], UPt_3 [30–32] and $(\text{U},\text{Th})\text{Be}_{13}$ [33], and $\text{Lu}_5\text{Rh}_6\text{Sn}_{18}$ [34] and even elemental rhenium [20], while for a large number of NCS superconductors, time-reversal symmetry is preserved [7]. This leaves open the important question of how the occurrence of time-reversal symmetry breaking, the crystallographic structure (NCS or CS), and the nature of the superconducting pairing mechanism are related to one another.

In this paper we discuss the properties of La_7Pd_3 which is one of a group of hexagonal NCS superconductors with a Th_7Fe_3 -type structure (space group $P6_3mc$). By investigating the superconducting ground state of La_7Pd_3 using muon spectroscopy further insight can be gained into the unusual superconducting behavior of this group of intermetallic compounds. Pedrazzini *et al.* previously reported some of the superconducting and normal-state properties of La_7Pd_3 as well as other members of this group of superconductors, however, the fact that this family of materials has a noncentrosymmetric structure was not emphasized [35]. Here, the superconducting and normal-state properties of La_7Pd_3 are investigated using magnetization, heat capacity, and resistivity measurements. Transverse-field muon spin rotation data are presented that indicate La_7Pd_3 has a conventional s -wave

* d.mayoh.1@warwick.ac.uk

† m.r.lees@warwick.ac.uk

superconducting gap symmetry. Zero-field muon spin relaxation curves provide evidence of time-reversal symmetry breaking in La_7Pd_3 . Finally, we compare our results on La_7Pd_3 with those obtained for other La_7X_3 superconductors and the Re-based α -Mn superconductors.

II. EXPERIMENTAL DETAILS

Polycrystalline samples of La_7Pd_3 were prepared from stoichiometric quantities of La (3N) and Pd (3N) in an arc furnace under an argon atmosphere on a water-cooled copper hearth. The sample buttons were melted and flipped several times to ensure phase homogeneity. The observed weight loss during the melting was negligible. The sample buttons were then sealed in an evacuated quartz tube, and annealed for 5 days at 500 °C. The material is air sensitive and was observed to rapidly develop an orange surface discoloration if exposed to air. The samples were stored in a glove-box under an argon atmosphere. A Quantum Design Physical Property Measurement System was used to measure both the heat capacity and electrical resistivity between 1.8 and 300 K in applied fields up to 9 T. A Quantum Design He-3 insert was used to access temperatures down to 0.5 K. A Quantum Design Magnetic Property Measurement System with iQuantum He-3 insert was used to measure the magnetization between 0.5 and 300 K in applied fields up to 7 T. Muon spin relaxation/rotation (μSR) measurements were performed using the MuSR spectrometer at the ISIS Neutron and Muon Source at the Rutherford Appleton Laboratory, UK μSR measurements were performed in both transverse-field (TF) and zero-field (ZF) modes. A full description of the detector geometries can be found in Ref. 36. A crushed sample of La_7Pd_3 was mounted on a 99.995% silver plate and inserted into a dilution refrigerator to measure at temperatures from 50 mK to 4 K.

III. CHARACTERIZATION

A. Magnetization and electrical resistivity measurements

To confirm bulk superconductivity in the La_7Pd_3 samples the dc volume magnetic susceptibility as a function of temperature, $\chi_{\text{dc}}(T)$, was measured in an applied field of 1.2 mT between 0.5 and 1.7 K as shown in Fig. 1(a). A rectangular sample of La_7Pd_3 was cut from the sample button to give a well-defined shape with a demagnetization factor $N = 0.13$ [37]. A sharp change in the susceptibility marks the onset of superconductivity in La_7Pd_3 at $T_{\text{c}}^{\text{onset}} = 1.46(5)$ K in excellent agreement with a previous report [35]. Between 0.5 and 1.1 K a full Meissner fraction ($\chi_{\text{dc}} = -1$) is clearly visible indicating bulk superconductivity in La_7Pd_3 . Several magnetization versus field loops were collected at different temperatures from

0.5 to 1.5 K in fields up to 10 mT. The lower critical field is estimated by measuring the field at which the flux first enters the sample, the first deviation from linearity in the magnetization versus applied field [38]. Figure. 1(b) shows the lower critical field values extracted from these magnetization versus field loops. The temperature dependence of $H_{\text{c1}}(T)$ can be described by the Ginzburg-Landau (GL) formula $H_{\text{c1}}(T) = H_{\text{c1}}(0) [1 - t_r^2]$, where $t_r = T/T_{\text{c}}$, giving $\mu_0 H_{\text{c1}}(0) = 6.9(2)$ mT. The magnetic susceptibility in the normal state shown in Fig. 2 is almost temperature independent between 300 and 5 K with a shallow minimum at ~ 50 K. An upturn in $\chi(T)$ below 5 K is consistent with the presence of a small quantity of paramagnetic impurities (other rare-earths with sizable localized magnetic moments) present in the La used to prepare the samples. The normal state behavior of $\chi(T)$ is qualitatively similar to the only previous report [35].

The temperature dependence of the electronic resistivity in La_7Pd_3 is shown in Fig. 2. The shape of $\rho(T)$ is characteristic of other NCS superconductors in the Th_7X_3 series [35] as well as many intermetallic materials [39, 40]. The resistivity at 300 K is $201.1(5) \mu\Omega \text{ cm}$ and the residual resistivity ρ_0 at 2 K, just above T_{c} , is $48.4(3) \mu\Omega$ giving a residual resistivity ratio of ~ 4.2 indicating poor metallic behavior. Using a simple Drude model [39, 41] we estimate the mean free path, $\ell = 12.4(1)$ nm.

B. Specific heat measurements

The temperature dependence of the heat capacity in La_7Pd_3 between 0.45 and 2.75 K is shown in Fig. 3(a). A sharp jump in the heat capacity, ΔC , is seen at $1.45(5)$ K indicating the onset of bulk superconductivity in La_7Pd_3 . The superconducting transition in La_7Pd_3 is typical of that seen in a type-II superconductor. The normal-state heat capacity at $T > 1.45$ K can be modeled using

$$C(T)/T = \gamma_{\text{n}} + \beta_3 T^2 + \beta_5 T^4, \quad (1)$$

to give the Sommerfeld coefficient $\gamma_{\text{n}} = 50.2(2)$ mJ/mol K² and $\beta_3 = 4.86(4)$ mJ/mol K⁴. Writing $\theta_{\text{D}} = \left(\frac{12\pi^4}{5} N k_{\text{B}}/\beta\right)^{\frac{1}{3}}$ gives the Debye temperature $\Theta_{\text{D}} = 159(2)$ K. The large γ_{n} is quite unusual for noncentrosymmetric superconductors, with the value for La_7Pd_3 surpassing some heavy-fermion superconductors such as CeCoGe_3 ($\gamma_{\text{n}} = 32$ mJ/mol K²) [42]. This suggests that there is an enhanced density of states at the Fermi level for La_7Pd_3 . This value of γ_{n} is consistent with that seen in other La_7X_3 [2, 3, 35, 43] compounds suggesting that this enhancement is a common feature of this group of superconductors.

The electronic heat capacity in zero applied field in the superconducting state can be used to look for evidence for an unusual superconducting order parameter. The

normalized entropy $S_{\text{el}}/\gamma_{\text{n}}T_{\text{c}}$ is written as

$$\frac{S_{\text{el}}(T)}{\gamma_{\text{n}}T_{\text{c}}} = -\frac{6}{\pi^2} \frac{\Delta(0)}{k_{\text{B}}T_{\text{c}}} \int_0^\infty [f \ln(f) + (1-f) \ln(1-f)] d\epsilon, \quad (2)$$

where $f(E) = [1 + \exp(E/k_{\text{B}}T)]^{-1}$ is the Fermi-Dirac distribution function with energy $E = \sqrt{\epsilon^2 + [\Delta(T)]^2}$. ϵ is the energy of the normal state electrons and $\Delta(T) = \Delta(0)\delta(T)$ where $\Delta(0)$ is the magnitude of the superconducting gap at zero kelvin and the temperature dependence of the energy gap is approximated using a single-gap BCS expression [44], $\delta(T) = \tanh\{1.82[1.018(T_{\text{c}}/T - 1)]^{0.51}\}$. The specific heat in the superconducting state is then calculated from [45]

$$\frac{C_{\text{el}}(T)}{\gamma_{\text{n}}T_{\text{c}}} = T \frac{d(S_{\text{el}}/\gamma_{\text{n}}T_{\text{c}})}{dT}. \quad (3)$$

Figure 3(b) shows that the normalized electronic heat capacity $C_{\text{el}}/\gamma_{\text{n}}T$ as function of the reduced temperature T/T_{c} . The data and the fit are in good agreement indicating that the material has an isotropic, largely s -wave superconducting gap. $\Delta C/\gamma_{\text{n}}T_{\text{c}} = 1.27(1)$ and $\Delta(0)/k_{\text{B}}T_{\text{c}} = 1.67(1)$ are both slightly lower than the 1.43 and 1.76, respectively, expected from the BCS theory in the weak-coupling limit. This may indicate a slightly diminished electron-phonon coupling strength in La_7Pd_3 , however, see Section IV.

C. Upper critical field calculations

Fig. 4(a) shows measurements of the resistivity as a function of temperature, $\rho(T)$, for La_7Pd_3 in various magnetic fields. There is a sharp superconducting transition at $T_{\text{c}} = 1.47(5)$ K with a width of $\Delta T = 0.05$ K in zero-applied field that is suppressed with increasing magnetic field. The transition also broadens, $\Delta T = 0.23(1)$ K at 450 mT. Measurements of resistivity as a function of magnetic field at fixed temperature were also performed. The T_{c} values determined from these data are included in Fig. 4(c). The temperature dependence of the heat capacity around the superconducting transition in different applied magnet fields is shown in Fig. 4(b). Again, the transition is suppressed and broadened with increasing magnetic field.

Values for the upper critical field, $H_{\text{c}2}$, of La_7Pd_3 were estimated from the midpoint of the superconducting transition in the resistivity data [see Fig. 4(a)] and the heat capacity data [see Fig. 4(b)]. Figure 4(c) shows the upper critical field values as a function of temperature. The $H_{\text{c}2}$ values exhibit a positive curvature close to T_{c} . This behavior can be captured by the Ginzburg-Landau phenomenological model for upper critical fields, $H_{\text{c}2}(T) = H_{\text{c}2}(0) [(1 - t_{\text{r}}^2)/(1 + t_{\text{r}}^2)]$, giving a good fit to the data and an estimated upper critical field $\mu_0 H_{\text{c}2}(0) = 652(5)$ mT, almost 2.5 times the previously reported value [35], but still well below the Pauli limit

which is similar to other superconductors in this series. Using $H_{\text{c}2}(0) = \frac{\Phi}{2\pi\xi^2}$ gives $\xi = 22.5(1)$ nm.

La_7Pd_3 contains lanthanum and palladium and so it is anticipated that there may be a significant spin-orbit coupling contribution to the physics of the superconducting state of La_7Pd_3 . The Werthamer-Helfand-Hohenberg (WHH) model allows for the inclusion of spin-orbit coupling in the upper critical field calculations [39, 46]. A fit to the $H_{\text{c}2}(T)$ data was attempted using the WHH model as shown by the orange dash-dotted line in Fig. 4(c) giving a slightly smaller $\mu_0 H_{\text{c}2}(0) = 620(3)$ mT. However, this model is unable to capture the curvature of the upper critical field values, cf. La_7Ir_3 where a WHH model provided a reasonable fit to the $H_{\text{c}2}(T)$ data [2].

IV. μSR MEASUREMENTS, THE SUPERCONDUCTING ORDER-PARAMETER, AND TIME-REVERSAL SYMMETRY BREAKING

The macroscopic superconducting state of La_7Pd_3 was probed using magnetization, resistivity, and heat capacity, however, in superconductors the microscopic magnetic environment formed by the vortex lattice can provide an essential insight into the superconducting state. Positive muons are an excellent probe of the local magnetic environment when implanted into a superconductor. The superconducting state of La_7Pd_3 has been investigated using transverse-field, longitudinal-field, and zero-field μSR .

Transverse-field spectra were collected at temperatures between 0.1 to 2.75 K in applied fields ranging from 10 to 50 mT, in the mixed state [$\mu_0 H_{\text{c}1}(0) = 6.9(2)$ mT]. In order to produce a well-ordered flux line lattice, the sample was field-cooled before collecting the data on warming. Figure 5 shows typical examples of the asymmetry spectra in the superconducting (0.1 K) and normal state (2.75 K). In the superconducting state, the muons depolarize quite rapidly due to the effects of the flux line lattice. A small amount of depolarization is still visible in the normal-state due to nuclear magnetic moments present in the sample. The oscillatory muon spectra can be fitted using a Gaussian function coupled with a cosinusoidal term for the muons implanted in the sample, and a simple cosinusoidal term for the muons implanted in the silver sample plate:

$$G_{\text{TF}}(t) = A_1 \exp\left(-\frac{\sigma^2 t^2}{2}\right) \cos(\gamma_{\mu} B_1 t + \phi) + A_2 \cos(\gamma_{\mu} B_2 t + \phi). \quad (4)$$

A_1 and A_2 are the sample and silver sample holder asymmetries, B_1 and B_2 are the average fields in the superconductor and silver plate, ϕ is the shared phase offset, $\gamma_{\mu}/2\pi = 133.5$ MHz T^{-1} is the muon gyromagnetic ratio and σ is the total depolarization rate. By fitting the spectra collected at different temperatures and fields us-

ing Eq. (4), the temperature dependence of σ can be determined as shown in Fig. 6(a). The total depolarization rate, σ , is related to the depolarization due to the flux line lattice, σ_{FLL} , and the nuclear moments, σ_{N} , by

$$\sigma^2 = \sigma_{\text{FLL}}^2 + \sigma_{\text{N}}^2. \quad (5)$$

The nuclear depolarization rate is found to remain constant over all temperatures at $\sigma_{\text{N}} = 0.162(1) \mu\text{s}^{-1}$. Since the upper critical field is comparable with the applied fields used in these measurements σ_{FLL} has a considerable field dependence. This is due to significant shrinking of the inter vortex distances within the flux line lattice as the applied field is increased. The effect of the vortex cores and the expected field dependence of the second moment of the field distribution have been calculated using different models. From calculations based on the Ginzburg-Landau model the field dependence of σ_{FLL} can be described using

$$\sigma_{\text{FLL}} [\mu\text{s}^{-1}] = 4.854 \times 10^4 (1 - h_{\text{r}}) \times \{1 + 1.21 (1 - \sqrt{h_{\text{r}}})^3\} \lambda^{-2} [\text{nm}^2] \quad (6)$$

where $h_{\text{r}} = H/H_{\text{c}2}$ is the reduced field and λ^{-2} is the inverse square of the penetration depth [47]. By taking isothermal cuts of the data shown in Fig. 6(a) as denoted by the dashed line, Eq. (6) can be used to fit to the data, as shown in Fig. 6(b), and the penetration depth can be extracted. The resulting temperature dependence of λ^{-2} , which reflects the variation in the superfluid density, is shown in Fig. 6(b) and this can be used to investigate the nature of the superconducting gap in La_7Pd_3 . In the clean limit, the magnetic penetration depth can be modeled using

$$\frac{\lambda^{-2}(T)}{\lambda^{-2}(0)} = 1 + 2 \int_{\Delta(T)}^{\infty} \left(\frac{\partial f}{\partial E} \right) \frac{E dE}{\sqrt{E^2 - \Delta^2(T)}}, \quad (7)$$

where f is the Fermi-Dirac distribution function and the temperature dependence of the gap for an isotropic s -wave model is $\Delta(T) = \Delta(0) \delta(T)$ as in Section III B. The fit produced by this model is shown by the dashed line in Fig 6(c). The penetration depth at zero kelvin was calculated to be $\lambda(0) = 495(4) \text{ nm}$. The value of $\Delta(0) = 0.30(4) \text{ meV}$ obtained gives $\Delta(0)/k_{\text{B}}T_{\text{c}} = 2.40(13)$ which is above both the BCS value of 1.76 and the value determined from the heat capacity measurements. Differences in $\Delta(0)/k_{\text{B}}T_{\text{c}}$ determined from heat capacity and μSR data have been observed in other superconductors, e.g. [48]. Possible reasons for the difference include multi-gap superconductivity, a gap anisotropy, or a nodal gap due to a small triplet component leading to a reduced anomaly in heat capacity at T_{c} [49–51].

Zero-field measurements were performed on La_7Pd_3 to look for evidence of time-reversal symmetry breaking in the superconducting state. Examples of the asymmetry spectra collected at temperatures above (2.75 K) and below (0.1 K) the superconducting transition are shown

in Fig. 7(a). These spectra exhibit considerable relaxation. The absence of any oscillatory component in the signals rules out the possibility of there being magnetic ordering in the sample. This observation is supported by measurements of the temperature dependence of the magnetic susceptibility at magnetic fields above $H_{\text{c}2}(0)$ (see inset in Fig. 2). It can be assumed that the majority of the relaxation arises from the presence of static, randomly orientated nuclear moments, while the increased relaxation rate below T_{c} indicates the presence of additional small internal magnetic fields in the superconducting state. These small magnetic fields are associated with the onset of time-reversal symmetry breaking. To eliminate any possibility of the relaxation coming from spin fluctuations a small longitudinal field (LF) of 5 mT was applied, as shown in Fig. 7(a). The complete decoupling of the muons from the proposed relaxation channel in this small LF indicates that the spontaneous magnetic fields are static or at least quasi-static over the lifetime of the muon.

The response of the muons to the nuclear moments can be captured using the Kubo-Toyabe expression

$$G_{\text{KT}}(t) = \frac{1}{3} + \frac{2}{3} (1 - \sigma_{\text{ZF}}^2 t^2) \exp\left(-\frac{\sigma_{\text{ZF}}^2 t^2}{2}\right), \quad (8)$$

where σ_{ZF} measures the width of the nuclear dipolar field experienced by the muons. The asymmetry can then be modeled by

$$G(t) = A_0 G_{\text{KT}}(t) \exp(-\Lambda t) + A_{\text{bg}}, \quad (9)$$

where A_0 and A_{bg} are the sample and background asymmetries, respectively, and Λ measures the electronic relaxation rate. The sample and background asymmetries were found to be constant at all temperatures. σ_{ZF} was found to decrease linearly with increasing temperature from 0.1 to 2.75 K across T_{c} [see Fig. 7(c)] while Λ was found to be temperature independent above the superconducting transition and to increase immediately below T_{c} at $\sim 1.2 \text{ K}$ [see Fig. 7(b)].

The increase in Λ occurs at a temperature slightly below the superconducting transition temperature as determined from magnetization, resistivity, heat capacity, and TF- μSR measurements. This temperature difference between the signal marking the onset of TRS breaking and T_{c} is also seen in both La_7Ir_3 [1] and La_7Rh_3 [3], two other members of this group of materials, as well as other superconductors such as $\text{PrPt}_4\text{Ge}_{12}$ [26].

V. COMPARISONS WITH OTHER SUPERCONDUCTORS EXHIBITING TRSB

Magnetization, heat capacity, resistivity, and μSR measurements reveal that La_7Pd_3 is type-II superconductor with a $T_{\text{c}} = 1.45(5) \text{ K}$. Some of the fundamental superconducting parameters determined from these measurements are summarized in Table I. Heat capacity and

transverse-field μ SR measurements indicate that the superconducting order parameter in La_7Pd_3 is dominated by a BCS-like s -wave component. The temperature dependence of the upper critical field is well fitted by a Ginzburg-Landau model which provides further evidence of conventional superconducting behavior.

On the other hand, zero-field μ SR measurements reveal an increase in $\Lambda(T)$ at low temperature of $0.005(1) \mu\text{s}^{-1}$. This is taken as evidence for the onset of time-reversal symmetry breaking although this change in $\Lambda(T)$ is only visible below ~ 1.2 K. Similar behavior is observed in La_7Ir_3 and La_7Rh_3 (see Table II). It is possible that for all three materials TRS is broken at a second transition just below T_c . Such a scenario has been suggested for LaNiC_2 and LaNiGa_2 [50]. However, to date, there are no indications of any additional transition or evidence for two gap superconductivity in the La_7X_3 series of superconductors.

An increase in $\Lambda(T)$ at T_c in Sr_2RuO_4 [24], LaNiC_2 [17], and SrPtAs [52] is also attributed to time-reversal symmetry breaking. The $\Delta\Lambda$ and behavior of $\sigma_{\text{ZF}}(T)$ are given in Table II for comparison. In Sr_2RuO_4 , TRSB is thought to arise due to a degeneracy in the superconducting phase brought about by non-zero spin and orbital moments. This in turn allows for the creation of spontaneous moments near to grain boundaries and impurities due to variations in the superconducting order parameter [24, 27, 53]. In LaNiC_2 , the signature of TRSB results from hyperfine fields made by nonunitary spin triplet pairs [17]. LaNiC_2 and Sr_2RuO_4 have unconventional gap structures, while La_7Pd_3 , La_7Rh_3 , and La_7Ir_3 all appear to have BCS-like s -wave gaps. A spin-split Fermi surface can look conventional if the magnitude of the two superconducting order parameters are similar, and singlet-triplet pairing would be difficult to differentiate from conventional s -wave pairing if $\mathbf{d}(\mathbf{k})$ is small. In all the noncentrosymmetric compounds studied to date, the signature of TRSB is relatively weak when compared to the change in $\Lambda(T)$ seen in the p -wave superconductor Sr_2RuO_4 . Measurements on single crystals of La_7X_3 , which should more readily reveal any anisotropy or nodes in the gap, are essential to clarify the TRSB mechanism. The superconducting and normal-state properties of single crystal La_7Ni_3 point to it being a conventional superconductor [43], although no μ SR results have yet been published to confirm whether time-reversal symmetry breaking is present in La_7Ni_3 . This is important as the effects of spin-orbit coupling should be more prominent in La_7X_3 materials containing the heavier elements Ir, Pd, and Rh.

Similar challenges are faced by those investigating the properties of the Re-based α -Mn NCS superconductors. TRSB is reported for several compounds in this series, again with s -wave BCS-like gap structures [18–22, 39, 54–59] and rather small changes in $\sigma_{\text{ZF}}(T)$ (see Table II). The observation of time-reversal symmetry breaking in the centrosymmetric rhenium exhibiting type-II superconductivity is particularly interesting [22] and may indicate that TRSB in these Re-based compounds is not related to the noncentrosymmetric structure, cf. LaNiC_2 and LaNiGa_2 [17, 29]. Pristine rhenium is a type-I superconductor and is driven type-II by shear strain. It would be interesting to investigate whether the increase in defects that accompanies this strain plays any role in the TRSB, and whether other elemental superconductors, including in this context La, show any evidence for similar effects. Further studies of centrosymmetric La_7X_3 materials will also provide vital information on the role the crystallographic structure plays in time-reversal symmetry breaking. In particular, studies of the centrosymmetric La_7Ru_3 should indicate whether a lack of a center of inversion is necessary for time-reversal symmetry breaking in the La_7X_3 compounds.

VI. CONCLUDING REMARKS

Now that time-reversal symmetry breaking has been observed in La_7Pd_3 it joins the small number of NCS superconductors that also show this phenomena. Single crystals of these superconductors are required in order to distinguish parity mixing effects in the materials that appear to have predominantly s -wave BCS-like superconducting gap structures. Studies of elemental superconductors and centrosymmetric superconducting analogues are also needed to clarify how important properties such as the lack of an inversion center and inhomogeneities are in driving time-reversal symmetry breaking in NCS superconductors.

ACKNOWLEDGMENTS

We are thankful for the technical support provided by Ali Julian and Patrick Ruddy. This work is supported by UKRI and STFC through the provision of beam time at the ISIS Neutron and Muon source, UK. This work is funded by the EPSRC, United Kingdom, through grants EP/T005963/1 and EP/M028771/1.

-
- [1] J. A. T. Barker, D. Singh, A. Thamizhavel, A. D. Hillier, M. R. Lees, G. Balakrishnan, D. M. Paul, and R. P. Singh, *Phys. Rev. Lett.* **115**, 267001 (2015).
 - [2] B. Li, C. Q. Xu, W. Zhou, W. H. Jiao, R. Sankar, F. M. Zhang, H. H. Hou, X. F. Jiang, B. Qian, B. Chen, B. F.

- Bangura, and X. Xu, *Sci. Rep.* **8**, 651 (2017).
- [3] D. Singh, M. S. Scheurer, A. D. Hillier, D. T. Adroja, and R. P. Singh, *Phys. Rev. B* **102**, 134511 (2020).
- [4] E. Bauer and M. Sigrist, *Non-centrosymmetric Superconductors: Introduction and Overview* (Springer, Heidelberg).

- berg, 2012).
- [5] M. Sigrist, AIP Conf. Proc. **1162**, 55 (2009).
 - [6] M. Sigrist, S. Agterberg, P. Frigeri, N. Hayashi, R. Kaur, A. Koga, I. Milat, K. Wakabayashi, and Y. Yanase, J. Magn. Magn. Mater. **310**, 536 (2007).
 - [7] M. Smidman, M. B. Salamon, H. Q. Yuan, and D. F. Agterberg, Rep. Prog. Phys. **80**, 036501 (2017).
 - [8] E. Bauer, G. Hilscher, H. Michor, C. Paul, E. W. Scheidt, A. Griбанov, Y. Seropegin, H. Noel, M. Sigrist, and P. Rogl, Phys. Rev. Lett. **92**, 027003 (2004).
 - [9] Z. Sun, M. Enayat, A. Maldonado, C. Lithgow, E. Yelland, D. C. Peets, A. Yaresko, A. P. Schnyder, and P. Wühl, Nat. Commun. **6**, 6633 (2015).
 - [10] H. Q. Yuan, D. F. Agterberg, N. Hayashi, P. Badica, D. Vandervelde, K. Togano, M. Sigrist, and M. B. Salamon, Phys. Rev. Lett. **97**, 017006 (2006).
 - [11] M. Nishiyama, Y. Inada, and G.-Q. Zheng, Phys. Rev. Lett. **98**, 047002 (2007).
 - [12] H. Takeya, M. ElMassalami, S. Kasahara, and K. Hirata, Phys. Rev. B **76**, 104506 (2007).
 - [13] S. Harada, J. J. Zhou, Y. G. Yao, Y. Inada, and G.-Q. Zheng, Phys. Rev. B **86**, 220502(R) (2012).
 - [14] E. M. Carnicom, W. Xie, T. Klimczuk, J. Lin, K. Gornicka, Z. Sobczak, N. P. Ong, and R. J. Cava, Science Advances **4**, eaar7969 (2018).
 - [15] D. A. Mayoh, M. J. Pearce, K. Götze, A. D. Hillier, G. Balakrishnan, and M. R. Lees, J. Phys.: Condens. Matter **31**, 465601 (2019).
 - [16] D. A. Mayoh, A. D. Hillier, K. Götze, D. M. Paul, G. Balakrishnan, and M. R. Lees, Phys. Rev. B **98**, 014502 (2018).
 - [17] A. D. Hillier, J. Quintanilla, and R. Cywinski, Phys. Rev. Lett. **102**, 117007 (2009).
 - [18] R. P. Singh, A. D. Hillier, B. Mazidian, J. Quintanilla, J. F. Annett, D. M. Paul, G. Balakrishnan, and M. R. Lees, Phys. Rev. Lett. **112**, 107002 (2014).
 - [19] D. Singh, J. A. T. Barker, A. Thamizhavel, D. M. Paul, A. D. Hillier, and R. P. Singh, Phys. Rev. B **96**, 180501(R) (2017).
 - [20] T. Shang, M. Smidman, S. K. Ghosh, C. Baines, L. J. Chang, D. J. Gawryluk, J. A. T. Barker, R. P. Singh, D. M. Paul, G. Balakrishnan, E. Pomjakushina, M. Shi, M. Medarde, A. D. Hillier, H. Q. Yuan, J. Quintanilla, J. Mesot, and T. Shiroka, Phys. Rev. Lett. **121**, 257002 (2018).
 - [21] D. Singh, K. P. Sajilesh, J. A. T. Barker, D. M. Paul, A. D. Hillier, and R. P. Singh, Phys. Rev. B **97**, 100505(R) (2018).
 - [22] T. Shang, G. M. Pang, C. Baines, W. B. Jiang, W. Xie, A. Wang, M. Medarde, E. Pomjakushina, M. Shi, J. Mesot, H. Q. Yuan, and T. Shiroka, Phys. Rev. B **97**, 020502(R) (2018).
 - [23] S. K. Ghosh, M. Smidman, T. Shang, J. F. Annett, A. D. Hillier, J. Quintanilla, and H. Yuan, J. Phys.: Condens. Matter **33**, 033001 (2020).
 - [24] G. M. Luke, Y. Fudamoto, K. M. Kojima, M. I. Larkin, J. Merrin, B. Nachumi, Y. J. Uemura, Y. Maeno, Z. Q. Mao, Y. Mori, H. Nakamura, and M. Sigrist, Nature (London) **394**, 558 (1998).
 - [25] J. Xia, Y. Maeno, P. T. Beyersdorf, M. M. Fejer, and A. Kapitulnik, Phys. Rev. Lett. **97**, 167002 (2006).
 - [26] A. Maisuradze, W. Schnelle, R. Khasanov, R. Gumeniuk, M. Nicklas, H. Rosner, A. Leithe-Jasper, Y. Grin, A. Amato, and P. Thalmeier, Phys. Rev. B **82**, 024524 (2010).
 - [27] Y. Aoki, A. Tsuchiya, T. Kanayama, S. R. Saha, H. Sugawara, H. Sato, W. Higemoto, A. Koda, K. Ohishi, K. Nishiyama, and R. Kadono, Phys. Rev. Lett. **91**, 067003 (2003).
 - [28] L. Shu, W. Higemoto, Y. Aoki, A. D. Hillier, K. Ohishi, K. Ishida, R. Kadono, A. Koda, O. O. Bernal, D. E. MacLaughlin, Y. Tunashima, Y. Yonezawa, S. Sanada, D. Kikuchi, H. Sato, H. Sugawara, T. U. Ito, and M. B. Maple, Phys. Rev. B **83**, 100504(R) (2011).
 - [29] A. D. Hillier, J. Quintanilla, B. Mazidian, J. F. Annett, and R. Cywinski, Phys. Rev. Lett. **109**, 097001 (2012).
 - [30] G. M. Luke, A. Keren, L. P. Le, W. D. Wu, Y. J. Uemura, D. A. Bonn, L. Taillefer, and J. D. Garrett, Phys. Rev. Lett. **71**, 1466 (1993).
 - [31] P. D. de Reotier, A. Huxley, A. Yaouanc, J. Flouquet, P. Bonville, P. Impert, P. Pari, P. C. M. Gubbens, and A. M. Mulders, Phys. Lett. A **205**, 239 (1995).
 - [32] W. Higemoto, K. Satoh, N. Nishida, A. Koda, K. Nagamine, Y. Haga, E. Yamamoto, N. Kimura, and Y. Onuki, Physica. B **281-282**, 984 (2000).
 - [33] R. H. Heffner, J. L. Smith, J. O. Willis, P. Birrer, C. Baines, F. N. Gygax, B. Hitti, E. Lippelt, H. R. Ott, A. Schenck, E. A. Knettsch, J. A. Mydosh, and D. E. MacLaughlin, Phys. Rev. Lett. **65**, 2816 (1990).
 - [34] A. Bhattacharyya, D. T. Adroja, J. Quintanilla, A. D. Hillier, N. Kase, A. M. Strydom, and J. Akimitsu, Phys. Rev. B **91**, 060503(R) (2015).
 - [35] P. Pedrazzini, G. Schmerber, M. Gómez Berisso, J. P. Kappler, and J. G. Serni, Physica C **336**, 10 (2000).
 - [36] W. H. Lee, H. K. Zeng, Y. D. Yao, and Y. Y. Chen, Physica C **266**, 138 (1996).
 - [37] A. Aharoni, J. Appl. Phys. **83**, 3432 (1998).
 - [38] A. Umezawa, G. W. Crabtree, J. Z. Liu, T. J. Moran, S. K. Malik, L. H. Nunez, W. L. Kwok, and C. H. Sowers, Phys. Rev. B **38**, 2843 (1988).
 - [39] D. A. Mayoh, J. A. T. Barker, R. P. Singh, G. Balakrishnan, D. M. Paul, and M. R. Lees, Phys. Rev. B **96**, 064521 (2017).
 - [40] B. Joshi, A. Thamizhavel, and S. Ramakrishnan, Phys. Rev. B **84**, 064518 (2011).
 - [41] N. W. Ashcroft and N. D. Mermin, *Solid State Physics* (Holt, Rinehart and Winston, New York, 1976).
 - [42] R. Settai, I. Sugitani, Y. Okuda, A. Thamizhavel, M. Nakashima, Y. Onuki, and H. Harima, J. Magn. Magn. Mater. **310**, 844 (2007).
 - [43] A. Nakamura, F. Honda, Y. Homma, D. Li, K. Nishimura, M. Kakihana, M. Hedo, T. Nakama, Y. Onuki, and D. Aoki, IOP Conf. Series: J. Phys: Conf. Series **807**, 052012 (2017).
 - [44] A. Carrington and F. Manzano, Physica C **385**, 205 (2003).
 - [45] D. Johnston, Supercon. Sci. Tech. **26**, 115011 (2013).
 - [46] N. R. Werthamer, E. Helfand, and P. C. Hohenberg, Phys. Rev. **147**, 295 (1966).
 - [47] E. H. Brandt, Phys. Rev. B **68**, 054506 (2003).
 - [48] P. K. Biswas, A. D. Hillier, M. R. Lees, and D. M. Paul, Phys. Rev. B **85**, 134505 (2012).
 - [49] A. A. Golubov, J. Kortus, O. V. Dolgov, O. Jepsen, Y. Kong, O. K. Andersen, B. J. Gibson, K. Ahn, and R. K. Kremer, J. Phys.: Condens. Matter **14**, 1353 (2002).
 - [50] Z. F. Weng, J. L. Zhang, M. Smidman, T. Shang, J. Quintanilla, J. F. Annett, M. Nicklas, G. M. Pang, L. Jiao, W. B. Jiang, Y. Chen, F. Steglich, and H. Q. Yuan, Phys.

- Rev. Lett. **117**, 027001 (2016).
- [51] A. P. Mackenzie and Y. Maeno, Rev. Mod. Phys. **75**, 657 (2003).
 - [52] P. K. Biswas, H. Leutkens, T. Neupert, S. T., C. Baines, G. Pascua, A. P. Schnyder, M. H. Fischer, J. Goryo, M. R. Lees, H. Maeter, F. Brückner, H. H. Klauss, M. Nicklas, P. J. Baker, A. D. Hillier, M. Sigrist, A. Amato, and D. Johrendt, Phys. Rev. B **87**, 180503(R) (2013).
 - [53] C. H. Choi and P. Muzikar, Phys. Rev. B **39**, 9664 (1989).
 - [54] M. A. Khan, A. B. Karki, T. Samanta, D. Browne, S. Stadler, I. Vekhter, A. Pandey, P. W. Adams, D. P. Young, S. Teknowijoyo, K. Cho, R. Prozorov, and D. E. Graf, Phys. Rev. B **94**, 144515 (2016).
 - [55] G. M. Pang, Z. Y. Nie, A. Wang, D. Singh, W. Xie, W. B. Jiang, Y. Chen, R. P. Singh, M. Smidman, and H. Q. Yuan, Phys. Rev. B **97**, 224506 (2018).
 - [56] K. Matano, R. Yatagai, S. Maeda, and G. Q. Zheng, Phys. Rev. B **94**, 214513 (2016).
 - [57] D. Singh, A. D. Hillier, A. Thamizhavel, and R. P. Singh, Phys. Rev. B **94**, 054515 (2016).
 - [58] B. Chen, Y. Guo, H. Wang, Q. Su, Q. Mao, J. Du, Y. Zhou, J. Yang, and M. Fang, Phys. Rev. B **94**, 024518 (2016).
 - [59] C. S. Lue, H. F. Liu, C. N. Kuo, P. S. Shih, J.-Y. Lin, Y. K. Kuo, M. W. Chu, T.-L. Hung, and Y. Y. Chen, Supercond. Sci. Technol. **26**, 055011 (2013).
 - [60] J. Chen, L. Jiao, J. L. Zhang, Y. Chen, M. Nicklas, F. Steglich, and H. Q. Yuan, New J. Phys. **15**, 053005 (2013).
 - [61] I. Bonalde, R. L. Ribeiro, K. J. Syu, H. H. Sung, and W. H. Lee, New J. Phys. **13**, 123022 (2011).

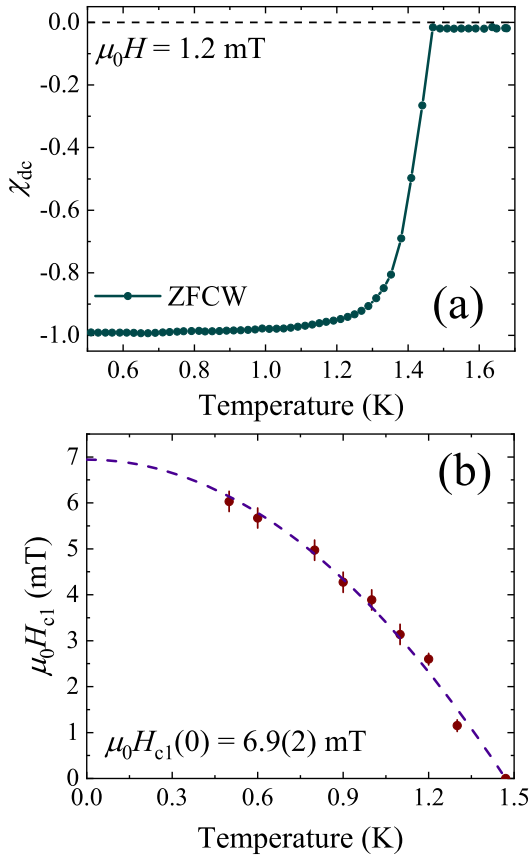


FIG. 1. (a) Temperature dependence of the dc volume magnetic susceptibility χ_{dc} for La_7Pd_3 , in zero-field-cooled warming (ZFCW) mode, measured in an applied magnetic field 1.2 mT showing a superconducting onset temperature $T_c^{\text{onset}} = 1.46(5)$ K. (b) Lower critical field H_{c1} versus temperature for La_7Pd_3 . The dashed line shows a fit to the data using $H_{c1}(T) = H_{c1}(0) [1 - t_r^2]$ which gives $\mu_0 H_{c1}(0) = 6.9(2)$ mT.

TABLE I. Superconducting parameters for La_7Pd_3 .

Parameter	Value	Unit
$\mu_0 H_{c1}(0)$	6.9(2)	mT
$\mu_0 H_{c2}(0)$	652(5)	mT
$\lambda(0)$	495(4)	nm
$\xi(0)$	22.5(1)	nm
κ_{GL}	22.0(3)	dim.

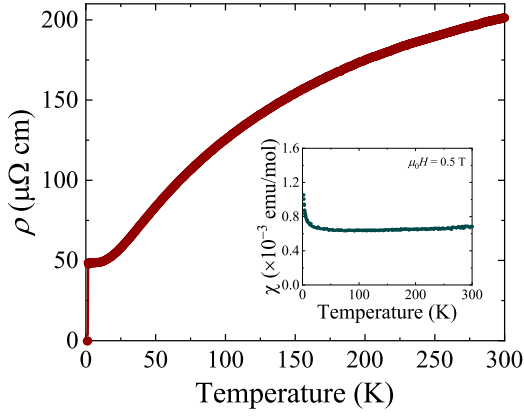


FIG. 2. Normal state properties of La_7Pd_3 : Temperature dependence of electronic resistivity from 1 to 300 K with zero applied magnetic field. The residual resistivity ratio (RRR) for La_7Pd_3 is approximately 4.2 and the residual resistivity just above the transition, $\rho_0(2\text{ K}) = 48.4(3)\ \mu\Omega\text{ cm}$. Inset: Temperature dependence of the magnetic susceptibility in an applied field of 0.5 T (in the normal state). An upturn at low temperature is consistent with the small quantity of paramagnetic impurities present in the La used to prepare the sample.

Compound	T_c (K)	$\Delta\Lambda$ (μs^{-1})	$\Delta\sigma$ (μs^{-1})	Channel of TRSB	Behavior of secondary channel	Instrument	Gap structure	CS or NCS	Ref.
La_7Pd_3	1.46	0.005	-	Λ	Linear inc.	MuSR	<i>s</i> -wave	NCS	This work.
La_7Ir_3	2.25	0.011	-	Λ	Linear inc.	MuSR	<i>s</i> -wave	NCS	1 and 2
La_7Rh_3	2.65	0.005	-	Λ	Linear inc.	MuSR	<i>s</i> -wave	NCS	3
Re_6Zr	6.75	-	0.008	σ	Constant	MuSR	<i>s</i> -wave	NCS	18, 39, 54–56
Re_6Hf	5.98	-	0.005	σ	Linear inc.	MuSR	<i>s</i> -wave	NCS	19, 57, and 58
Re_6Ti	6	-	0.009	σ	Linear dec.	MuSR	<i>s</i> -wave	NCS	21
$\text{Re}_{24}\text{Ti}_5$	6	0.006	-	Λ	Constant	GPS	<i>s</i> -wave	NCS	22 and 59
$\text{Re}_{0.82}\text{Nb}_{0.18}$	8.8	-	0.022	σ	-	MuSR, GPS, LTF	<i>s</i> -wave	NCS	20
Re	2.7	-	0.01	σ	-	GPS, LTF	<i>s</i> -wave	CS	20
LaNiC_2	2.7	0.009	-	Λ	Constant	MuSR		NCS	17, 60, and 61
LaNiGa_2	2.1	0.01	-	Λ	Constant	MuSR		CS	29
Sr_2RuO_4	1.5	0.04	-	Λ	-	M15	<i>p</i> -wave	CS	24

TABLE II. Selected properties of some noncentrosymmetric and centrosymmetric superconductors in which time-reversal symmetry breaking has been observed. $\Delta\Lambda$ and $\Delta\sigma$ are taken from the data presented in the listed references along with the channel in which the signal indicating TRS breaking is observed and the muon spectrometer used. These instruments include MuSR at ISIS, UK, the General Purpose Surface-Muon (GPS) and the Low Temperature Facility (LTF) instruments based at PSI, Switzerland, and the M15 beam line at TRIUMF, Canada.

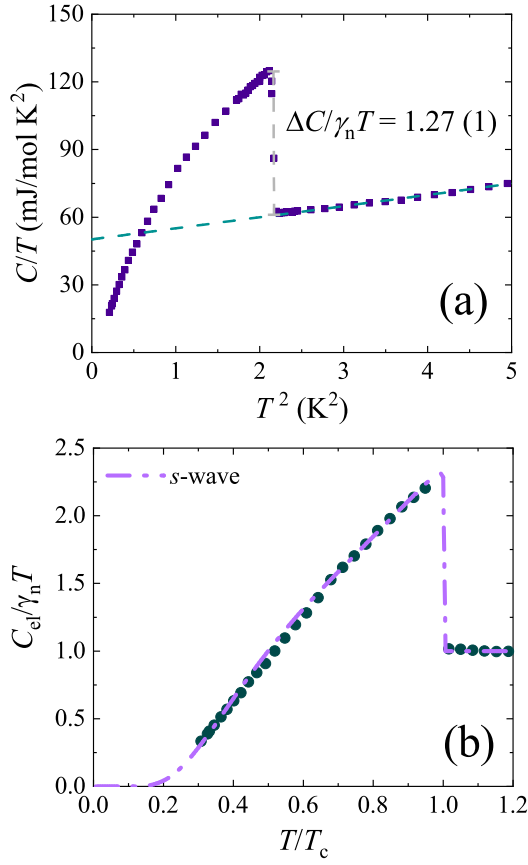


FIG. 3. (a) Temperature dependence of the zero-field heat capacity for La_7Pd_3 between 0.45 and 2.75 K showing a superconducting transition at $T_c = 1.45(5)$ K. The shape of the C versus T is indicative of a typical type-II superconductor. Fitting the data above T_c in the normal-state using Eq. (1) gives $\gamma_n = 50.2(2)$ mJ/mol K^2 . (b) Normalized electronic heat capacity $C_{\text{el}}/\gamma_n T$ versus the reduced temperature T/T_c in zero applied field. The dotted line shows a fit to the data for an isotropic s -wave gap made using Eqs. 2 and 3.

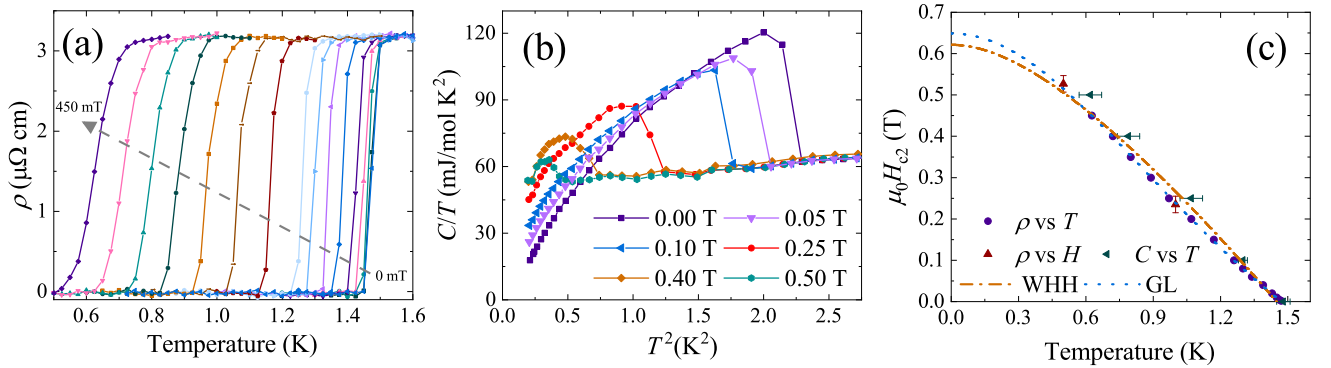


FIG. 4. (a) Temperature dependence of the resistivity of La_7Pd_3 showing the suppression and broadening of the resistive superconducting transition in applied fields from 0 to 450 mT. (b) C/T versus T^2 for La_7Pd_3 showing the suppression and broadening of the superconducting transition as the applied field is increased from 0 to 500 mT. (c) Temperature dependence of the upper critical field for La_7Pd_3 . The $H_{c2}(T)$ values were extracted from the midpoints of the anomalies in $C(T)/T$ and the midpoints of the resistive transitions. The dotted and dash-dotted lines show fits to the $\mu_0 H_{c2}(T)$ data using the GL and WHH models [39, 46], respectively.

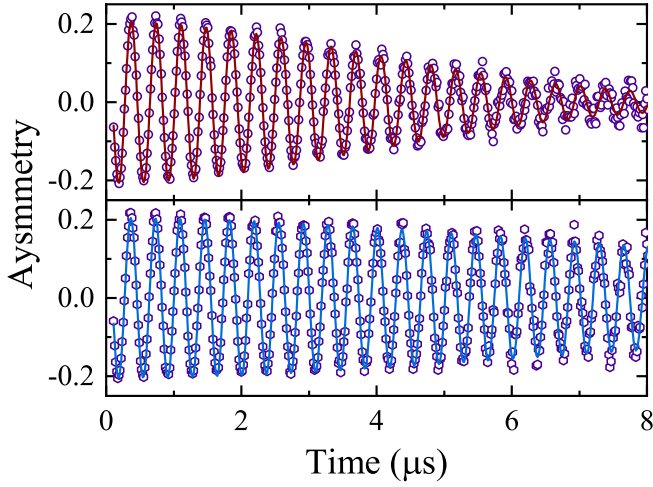


FIG. 5. Transverse-field μ SR spectra for La_7Pd_3 collected at 100 mK (top) and 2.25 K (bottom) in an applied magnetic field of 20 mT. The solid lines are fits to data using Eq. (4). Below the superconducting transition temperature the field distribution of the FLL causes the spectra to be significantly depolarized. Above the superconducting transition temperature the randomly oriented array of nuclear magnetic moments continue to depolarize the muons but at a reduced rate.

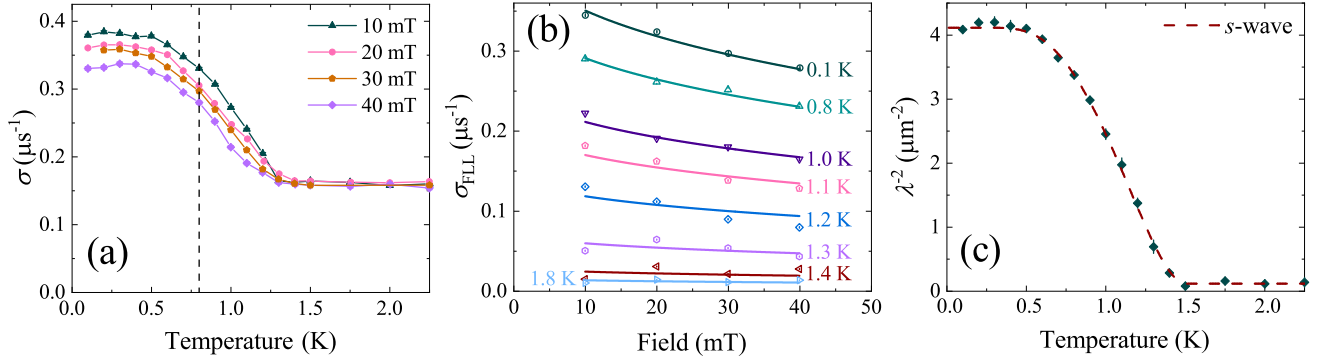


FIG. 6. (a) Temperature dependence of the total spin depolarization, σ , for La_7Pd_3 collected in fields between 10 and 50 mT. Isothermal cuts (the dashed line shows the cut made at 0.8 K) were used to calculate the field dependence of σ_{FLL} in La_7Pd_3 . (b) Field dependence of the muon spin relaxation due to the flux line lattice, σ_{FLL} , at different temperatures. The solid lines are fits to the data using Eq. (6). (c) Temperature dependence of the inverse square of the penetration depth, λ^{-2} . The dashed line is a fit to the data using Eq. (7).

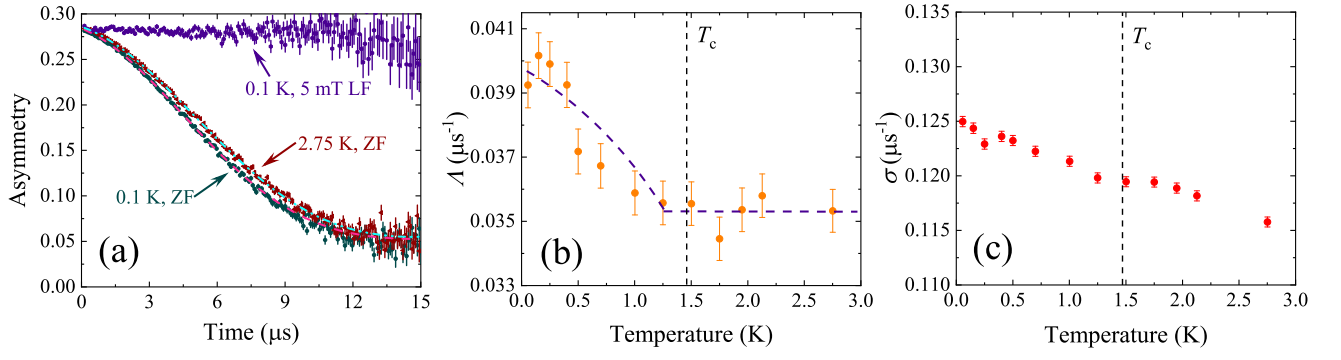


FIG. 7. (a) ZF and LF- μ SR spectra collected at 0.1 (green) and 2.75 K (red), the data is fit using the Gaussian Kubo-Toyabe model (dashed lines). (b) Temperature dependence of the electronic relaxation rate Λ can be seen to increase below 1.2 K just below T_c . (c) Temperature dependence of the nuclear relaxation rate σ shows no change at T_c .